Journal Name

RSCPublishing

ARTICLE

A Strategy to Reduce the Angular Dependence of a Dye-Sensitized Solar Cell by Coupling to a TiO_2 Nanotube Photonic Crystal

Cite this: DOI: 10.1039/xoxxoooooox

Received ooth January 2012,
Accepted ooth January 2012

DOI: 10.1039/xoxxoooooox

www.rsc.org/

Min Guo,[a] Keyu Xie,[*,b] Xiaolin Liu,[a] Yu Wang,[a] Limin Zhou[c] and Haitao Huang[*,a],

Almost all types of solar cells suffer from a decreased power output when the incident light is tilted away from normal since the incident intensity generally follows a cosine law of the incident angle. Making use of the blue shift nature of the Bragg position of a TiO2 nanotube photonic crystal (NT PC) under oblique incidence, we demonstrate experimentally that the use of the NT PC can partially compensate the cosine power loss of a dye-sensitized solar cell (DSSC). The strategy used here is to purposely choose the Bragg position of the NT PC to be at the longer wavelength side of the dye absorption peak. When the incident light is tilted, the blue shift of the Bragg position results in more overlap with the dye absorption peak, generating a higher efficiency that partially compensates the reduced photon flux due to light inclination. Moreover, the unique structure of the vertically aligned TiO2 nanotubes contributes an additional scattering effect when the incident light is tilted. As a result, the power output of a DSSC coupled with the NT PC layer shows a much flatter angular dependence than a DSSC without the NT PC. At all the incident angles, the DSSC coupled with the NT PC layer also shows a higher power conversion efficiency than the one without. The concept of using NT PC to mitigate the angular dependence of DSSCs can be easily extended to many other optoelectronic devices that are irradiance sensitive.

Introduction

To meet the crucial challenge of depleting fossil fuels, photovoltaics (PV) as one of the renewable energy sources are gradually being used on a global scale and in a variety of forms.[1-4] A common problem with all types of PVs is that they are irradiance sensitive which results in a decay of power output when the incident light is tilted. While a sophisticated sunlight tracking system may solve the problem, it is expensive and consumes energy. Although many light management techniques, such as the use of scattering layers, plasmonic nanometal, superstructures and photonic crystals,[5-8] can enhance the power conversion efficiency, they in general do make the power output of a solar cell less irradiance sensitive.

Integrating photonic crystal (PC) structures in photovoltaics, as an effective light trapping method, has gained increasing interest and led to significant enhancement of power conversion efficiencies in various types of solar cells, such as silicon solar cells,[9, 10] quantum dot-sensitized solar cells,[11, 12] perovskite-based solar cells,[13] organic solar cells,[14, 15] and dye-sensitized solar cells (DSSCs).[16] Typically, for PC based DSSCs, a bi-layered architecture consisting of an absorbing layer (normally ruthenium dye sensitized nanocrystalline TiO_2) and an additional underlying PC layer (such as SiO_2/TiO_2 multi-layers,[17-19] TiO_2 inverse opal layers,[20-22] and TiO_2 nanotube PC membranes[23, 24]) has been adopted to efficiently harvest the solar irradiation. The use of PC is regarded as a promising way to enhance light harvesting in DSSCs by confining or slowing down light at certain wavelength range, which are caused by several possible effects, i.e., reflecting the unabsorbed photons back to the absorbing layer, suppressing group velocities of photons and creating resonant modes.[25, 26] Particularly, for the TiO_2 nanotube PC (NT PC) coupled DSSCs, it has been demonstrated that light harvesting enhancement effect strongly depends on how well the Bragg reflection peak of the NT PC is matched to the dye absorption spectrum.[23,24]

Here, we propose a strategy to reduce the angular dependence of DSSCs by coupling the photoanodes to TiO_2 NT PC structures. The reduced angular dependence of the power output is resulted from two mechanisms: (1) The Bragg position of the NT PC is purposely chosen to be located at the longer wavelength side of the dye absorption peak. When the incident light is tilted, the Bragg peak will blue shift, having more overlap with the dye absorption peak, and hence harvest more efficiently the incident light that partially compensates the reduced photon flux due to light inclination; and (2) When the

incident light is tilted, the photons will encounter more interfaces between the walls of nanotubes and be scattered. The enhanced light scattering also compensates the power loss due to reduced photon flux. The angular dependence of the optical properties of the TiO_2 NT PC structure and its effect on the photovoltaic performance of the integrated solar cells has been systematically studied in the present work. The effect of the lattice constant of the NT PC structure on the suppression of the angular dependence of power output has been studied by both experimental measurements and theoretical simulations. It is found that the introduction of TiO_2 NT PC not only stabilizes the power output under oblique illumination, but also enhances light harvesting at all the incident angles studied. It is believed that the idea developed in the current work is also applicable to a variety of optoelectronic devices that are irradiance sensitive.

Experimental

Fabrication of TiO_2 NT PC

The TiO_2 NT PCs were synthesized by periodic current-pulse anodization following the same experimental procedure reported in our previous work.[24] By using different pulse durations and number of pulses, TiO_2 NT PCs with various lattice constants were obtained, namely, 120-NT PC, 150-NT PC, 190-NT PC and 230-NT PC (the number stands for the lattice constant in nanometers). In brief, ammonium fluoride (0.5 wt%) was dissolved to an aqueous EG solution (3 vol% DI water in EG) by stirring for 2h and used as electrolyte for all anodization processes. Unless stated otherwise, all the chemicals were purchased from International Laboratory (USA) and used as received. After 15 min's anodization at 60V in a two-electrode electrochemical cell, the titanium foils (99.7%, Strem Chemical) were ultrasonically processed and subsequently rinsed with DI water to remove the anodic TiO_2 nanotubes produced in this anodization step. In order to fabricate TiO_2 NT PC, a second anodization was carried out on the pre-treated titanium foil, using periodic current pulses with alternating high current density (so determined to obtain an anodization voltage of ~ 60V) and low current density (0A in this study). Different high current pulse durations (20, 30, 40 and 50s) were used to obtain NT PCs with different lattice constants (120, 150, 190 and 230nm, respectively) while the thicknesses of different NT PCs were kept at ~2.3μm. The as-anodized foil was further heat treated at 270°C for 1 h, followed by a third anodization at 60V for 2 h to remove the TiO_2 NT PC membrane from the Ti substrate. For comparison, TiO_2 NT membrane with similar thickness and nanotube diameter was also synthesized by a fixed voltage (60V) anodization in the second step.

Preparation and assembly of DSSCs

The materials for constructing DSSCs, including TiO_2 nanoparticle (NP) paste (13nm), FTO glass (Nippon Sheet Glass), Pt-coated FTO glass, thermal adhesive film (25μm thick, Surlyn-1702), N719 dye (Solaronix) and the electrolyte (DMPD: 1.0M, LiI: 0.1M, 4-TBP: 0.5M, I2: 0.12M, 3-methoxy propionitrile) were purchased from Wuhan Geao Instruments Science and Technology Co. Ltd (China). The photoanode was fabricated by adhering TiO_2 NT PC membranes on to the FTO substrate which had already been coated with a TiO_2 NP paste layer, using a doctor-blade method.[24] After annealing at 450°C for 3h with heating and cooling rates of 1°C • min^{-1}, the photoanodes were immersed in 0.3mM N719 dye (cis-bis(isothiocyanato)-bis(2,20-bipyridyl-4,-40-dicarboxylate) dissolved in ethanol at 60°C for 24h. The excess dye was washed away with ethanol. For comparison, TiO_2 NP photoanodes were also prepared as a reference in this study. A thermal adhesive film was used as a spacer to be sandwiched between the photoanode and a Pt counter electrode. The single cell is completed by infiltrating the liquid electrolyte into the cavity of the active area of cell and sealing with UV epoxy. For each type of the cells, more than 4 samples were fabricated and characterized.

Characterization of the photoanodes and DSSCs

The microstructures of the NT PCs and photoanodes were observed by field emission scanning electron microscope (FESEM, JEOL JSM-6335F). The optical properties of the photoanodes were characterized by a UV-Vis spectrophotometer (Model UV-2550, Shimadzu, Japan), with a sample rotation holder for angular measurements. The I-V curves were measured with a Newport 91160 solar-light simulator with an AM 1.5 filter. The incident light power was calibrated using a silicon photodiode previously calibrated at 100mW • cm^{-2}. In order to avoid spurious light influence, a black mask was used to wrap around the TiO_2 electrode and its lateral sides. The incident photon-to-current efficiency (IPCE) was recorded by a Newport 2931-C power meter, as a function of wavelength from 400 to 800nm (tuned with a Newport 74125 monochromator) with the light source from a Newport 66902 solar simulator. The light intensity was measured with a Newport 2931-C power meter equipped with a 71675_71580 detector probe. For the photovoltaic characterization under titled sunlight, sample rotation holder was used again.

Simulation and theoretical calculation

Finite-element full wave simulation was employed for both the reflection and absorption spectra simulation. In the model, the incoming light first incident on the conductive transparent substrate (refractive index=1.45). Then it successively passes through a 10-μm-thick TiO_2 NP layer with 50% porosity (the effective refractive index n_{np}=2.03), the TiO_2 NT PC or NT layer with a thickness ~ 2.3μm (the refractive index n_{TiO2}=2.51), and finally reach the electrolyte with a refractive index $n_{electrolyte}$=1.403, corresponding to propionitrile electrolyte.[25] The refractive indices of TiO_2 NP layer were calculated by the effective medium theory, assuming that the electrolyte fills all the pores. The NT PC and NT layers were modeled in a hexagonal lattice with the geometry similar to the experimental samples and the NTs arranged in the electrolyte with the axial direction of the NTs perpendicular to the cell surface. All TiO_2

layers, including NP, NT, and NT PC, were sensitized by ruthenium dye, whose absorption coefficient is obtained by fitting the photocurrent and the absorptance spectra of similar layer and device and is represented by the frequency-dependent imaginary part of the refractive index. Finally, the estimated photocurrent enhancement ΔJ_{sc} was calculated by using the following equation,[27]

$$\Delta Jsc = \frac{\int[LHE_{pc}(\lambda)]F(\lambda)d\lambda - \int[LHE_{ref}(\lambda)]F(\lambda)d\lambda}{\int[LHE_{ref}(\lambda)]F(\lambda)d\lambda} \quad (1)$$

where LHE_{pc} and LHE_{ref} are the light harvesting efficiencies of the NT PC based DSSC and the reference cell, respectively, which are defined as the fraction of incident light intensity absorbed by the dye in the devices. $F(\lambda)$ is the photon flux as a function of wavelength λ, which is calculated from the standard AM1.5G solar spectral irradiance.[28]

Results and discussion

The designed architecture of the NT PC based solar cells, consisting of a 10-μm-thick TiO_2 nanoparticle (NP) layer and a thin TiO_2 NT PC layer with the thickness around 2.3μm, is illustrated in Figure 1a and b. In this architecture, the thick TiO_2 NP works as the absorbing layer and the thin TiO_2 NT PC layer works as a Bragg mirror to reflect the unabsorbed photons back to the absorbing layer. In order to reveal the interplay between the angular optical properties of the NT PC and the photovoltaic properties of the integrated devices, NT PCs with four lattice constants, i.e., 120, 150, 190 and 230 nm, were produced by periodic current-pulse anodization and subsequently coupled to the TiO_2 NP layer, as shown in Figures 1b-f. The Bragg positions of the NT PCs with the three longest lattice parameters were located in the visible range, at about 450, 550, and 640 nm, respectively. For comparison, a reference cell consisting of only a TiO_2 NP layer (~12μm in thickness) and a TiO_2 NT/NP cell with a smooth nanotube layer instead of the NT PC layer (of similar thickness), are shown in Figure S1.

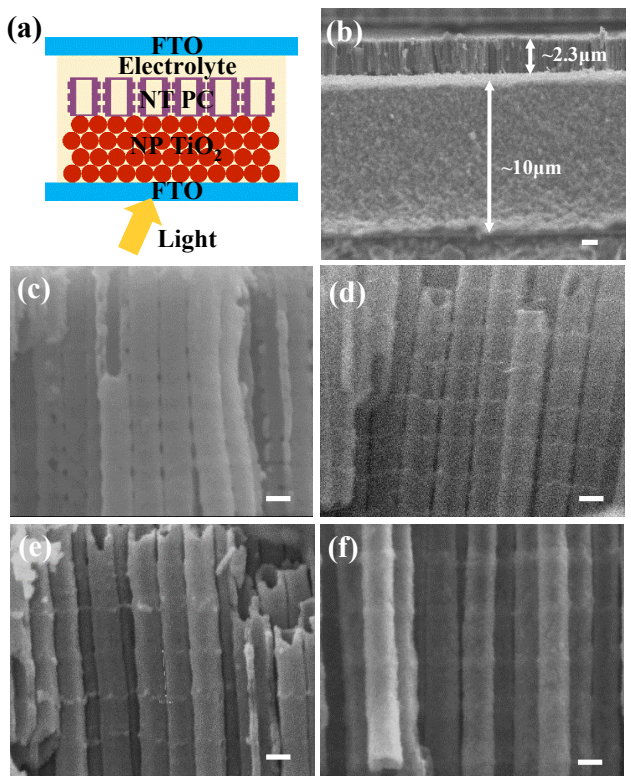

Fig. 1 (a) Schematic structure of DSSC based on the TiO_2 NT PC/TiO_2 NP photoanode. (b) Cross-sectional SEM image of the TiO_2 NT PC/TiO_2 NP photoanode. (c-f) Cross-sectional SEM images of NT PCs with different lattice constants: (c) 120nm, (d) 150nm, (e) 190nm, and (f) 230nm. The scale bar measures 100 nm.

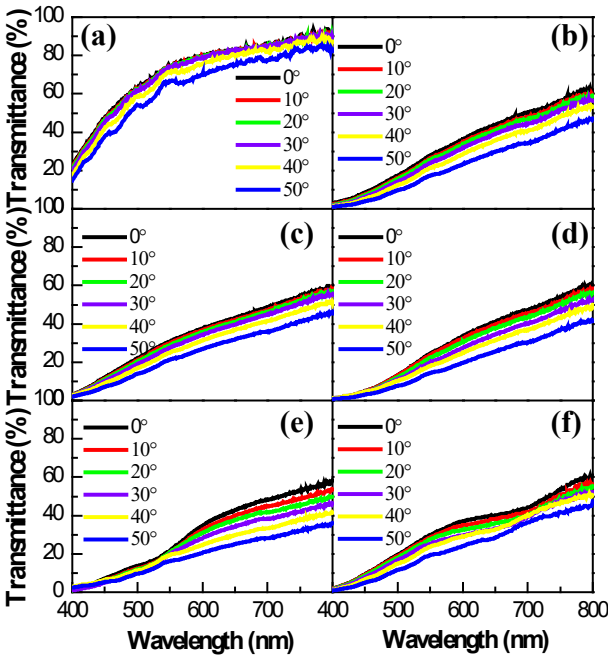

Fig. 2 Experimental transmission spectra of studied photoanodes under varying incident angles from 0 to 50°, (a) the TiO_2 NP based photoanode, (b) the TiO_2 NT/TiO_2 NP based photoanode, and the photoanodes based on TiO_2 NT PCs with different lattice constants: (c) 120 nm, (d) 150 nm, (e) 190 nm, and (f) 230 nm.

To investigate the effect of both the smooth NT and the NT PC on the angle dependent optical properties of the photoanode, the transmittance spectra of various types of photoanodes were characterized in air and under varying incident angles from 0 to 50°, as shown in Figure 2. The tilting of the incident angle is found to shift the absorption edge to a shorter wavelength for all NT PCs, which is consistent with the blue shift of the Bragg position, as seen from the simulated reflectance spectrum (Figure S2 a-d). According to the Bragg's law, $\lambda_{peak}=2dn_{eff}\sin\theta$ (where d is the lattice constant of the NT PC, n_{eff} is the effectiverefractive index, and θ is the angle between the incident light and the periodic planes),[29] the Brag peak λ_{peak} should blue shift as the incident angle increases (incident angle=90°−θ). This phenomenon can be easily observed by naked eyes, as shown in Figure S3, where the color of the photoanode turns from green to dark purple when the photoanode is tilted at a large angle. It also noted, according to

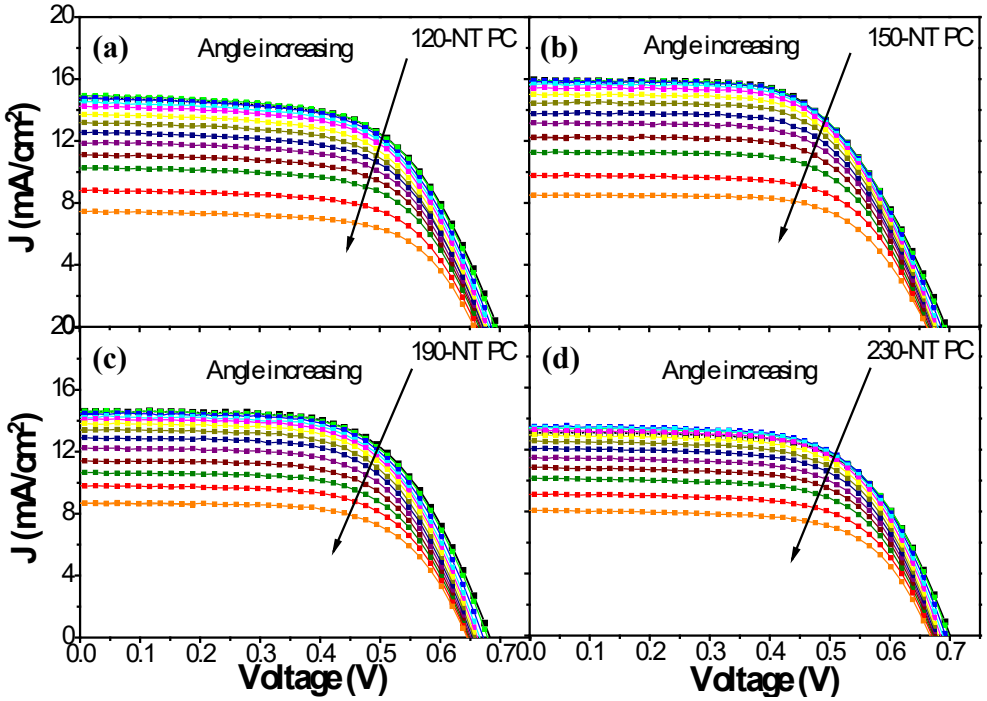

Fig. 3 The evolution of photocurrent-voltage curves of DSSCs made of a 10 μm-thick TiO2 NP electrode coupled to different TiO2 NT PCs: (a) 120-NT PC, (b) 150-NT PC, (c) 190-NT PC, (d) 230-NT PC, as the incident angle increases from 0 to 60°, in a step of 5°

the Bragg's law, the peak shift is more significant as d is increased (~45, 65 and 75 nm for 150-NT PC, 190-NT PC, 230-NT PC, respectively, calculated from Figure S2), implying a stronger angular dependence of the optical properties of the devices under longer lattice constant. In addition, since the Bragg position of the 120-NT PC locates in the ultraviolet range and shifts to even shorter wavelength when the sample is tilted, no visible wavelength shift of the 120-NT PC/TiO_2 NP photoanode can be seen in Figure 2c.

At the same time, the transmittance of all photoanodes gradually decreases as the sample is tilted, which is the consequence of stronger reflectance at the air-glass interface. However, it can also be seen from Figure 2 that, comparing to the TiO_2 NP based photoanode, the decline in transparency of the TiO_2 NT PC/TiO_2 NP and TiO_2 NT/TiO_2 NP photoanodes is more significant as the sample is titled. This is attributed to the additional enhanced diffuse scattering from the walls of nanotubes when the light is deviated from the axial direction of the nanotubes. This result agrees well with the simulated reflectance spectra of TiO_2 NT photoanode (Figure S2e), where the oscillation of reflection spectrum becomes stronger in intensity with increasing incident angles. It is believed that this unique scattering effect of NTs will assist the PC structure to compensate energy loss due to the tilting of incident sunlight.

In order to demonstrate the angular effect of TiO_2 NT PCs on the photovoltaic performance of the assembled cells under different incident angles, the photocurrent vs. voltage curves were measured under simulated sunlight of AM1.5G, as shown in Figure 3. It can be seen that under different incident angles, the curve shapes are similar with slightly changed open circuit voltages and fill factors, whereas the short circuit current, J_{sc}, of all the cells decreases with incident angles due to the reduced incident irradiation, $I_\theta = I_0 cos\theta$ (where I_θ is the incident intensity of sunlight at an incident angle θ)[19, 30] The I-V curves of TiO_2 NP based reference cell and TiO_2 NT/TiO_2 NP cell are also displayed in Figure S4. A careful examination shows that, although in general J_{sc} decreases with increasing incident angles for all the cells, the decreasing trends are different for cells coupled with different TiO_2 NT PCs, indicating a complex angular response of the integrated cells.

To clarify the angular response of the photocurrent efficiency of the solar cells based on different types of photoanodes, a detailed analysis on the variation of J_{sc} as a function of incident angle (0-60°) is conducted in Figure 4a. It can be seen that the introduction of NT PC increases the photocurrent for all the

measured incident angles from 0 to 60°. Under normal incidence, the preferred PC structure to get the maximum photocurrent is 150-NT PC, which is consistent with our previous work, and the photocurrent enhancement effect has been ascribed to the strong overlap between the Bragg reflection peak of the NT PC and the absorption peak of the dye.[23, 24] However, when the incident angle is increased, the difference in photocurrent enhancement among different cells becomes smaller. Figure 4b shows the normalized J_{sc} (normalized with respect to the short circuit current under normal incidence). It can be seen that, as compared to the TiO_2 NP reference cell and the cosine loss curve, the J_{sc} drop due to increased incident angle becomes less for the TiO_2 NT cell, which is attributed to the additional scattering effect of nanotubes when the incoming light deviates away from the axial direction of NTs. Such a drop in photocurrent can be further suppressed by the introduction of 190-NT PC or 230-NT PC, whose Bragg peak is located on the red side of the dye absorption peak. As the incident angle is increased, the Bragg peak blue shifts and results in an increased overlap with the dye absorption peak, inducing a greater percentage enhancement in photocurrent (Figure 4c). This photocurrent compensation effect makes the photovoltaic performance of the cells less sensitive to the variation of the sunlight incident angle, an attractive feature for practical applications of all types of solar cells. In other words, for a given allowable variation of power output, the working range of the incident angle is widened. For example, if a 20% drop in photocurrent is allowed in a practical application, the working range of the incident angle is 0-40° for the reference TiO_2 NP cell, while it is 0-50° for the 230-NT PC cell (Figure 4b). For the case of 120-NT PC and 150-NT PC, whose Bragg peak will move away from the dye absorption peak with increasing incident angles, the photocurrent compensation effect is mainly contributed by the increasing scattering effect of the NTs. The unique combination of the PC and the scattering effects of the NT PC structure allows us to have a better design of the photoanode structure for a more stable power output of solar cells under tilted sunlight, an important issue to be considered for practical applications.

The photocurrent compensation effect can be further revealed by Figure 4c, which illustrates the angular evolution of photocurrent enhancement, ΔJ_{sc}, of different types of NT and NT PC based solar cells, as compared to the NP reference cells. It can be found that the 190-NT PC and 230-NT PC cells have the most significant angular dependence of ΔJ_{sc}, due to both the PC effect (blue shift of the Bragg peak to have more overlap with the dye absorption peak) and the scattering effect. While for the 120-NT PC and 150-NT PC cells, ΔJ_{sc} is less sensitive to the incident angles due to the decaying PC effect, i.e., the Bragg peak is blue shifted to have less overlap with the dye absorption peak. A moderate angular dependence of ΔJ_{sc} is found in the TiO_2 NT cell since there is only the scattering effect, no PC effect.

The power conversion efficiency shows similar evolution to that of J_{sc}, as shown in Figure S5, with minor deviations caused by slightly and oppositely changed open circuit voltage and fill factor with respect to the incident angles (Figure S6).

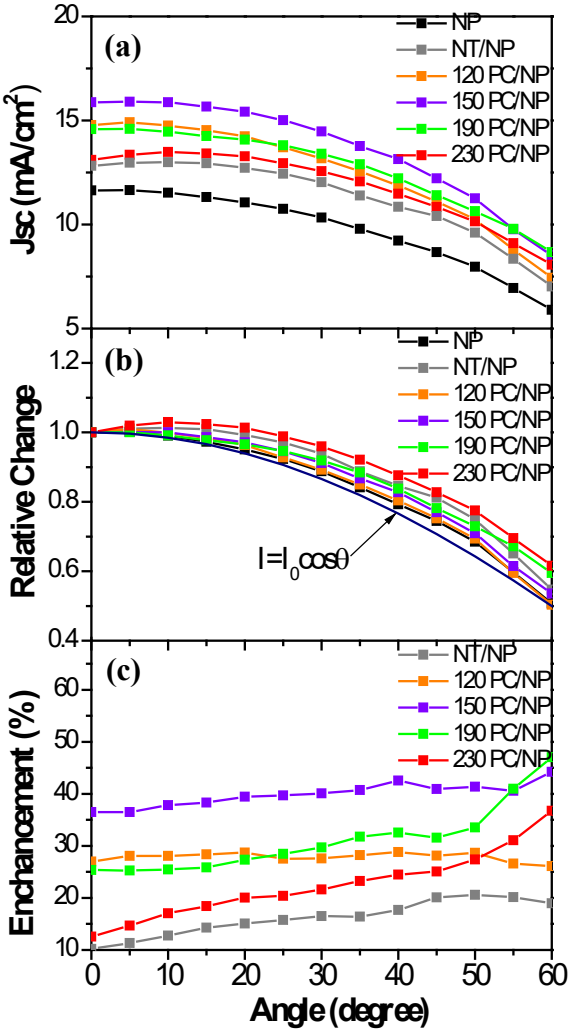

Fig. 4 Angular dependence of (a) J_{sc}, (b) normalized J_{sc} and cosine curve (dark blue line), and (c) J_{sc} enhancement (as compared to the reference cell) for different types of cells.

The origin and underlying mechanism of the angular dependence of the photocurrent enhancement effect of NT PCs can be further visualized and confirmed in the simulated absorptance spectra and the experimental incident photo-to-electron conversion efficiency (IPCE). Two incident angles, 0 and 50° are compared in Figure 5. Two different effects, namely, the Bragg mirror effect of PC and the scattering effect of the wall of NT, will play their roles in the photocurrent enhancement. Specifically, for 120-NT PC and 150-NT PC, whose Bragg position is located at the short wavelength side or very close to the dye absorption peak under normal incidence, the tilting of incident angle will shift the Bragg position to even shorter wavelength and hence increase the IPCE on the blue side of the dye absorption peak. For 190-NT PC and 230-NT PC, the tilting of incident angle will move the Bragg position closer to the dye absorption peak and hence increase the IPCE on the red side. In contrast, the scattering effect the walls of

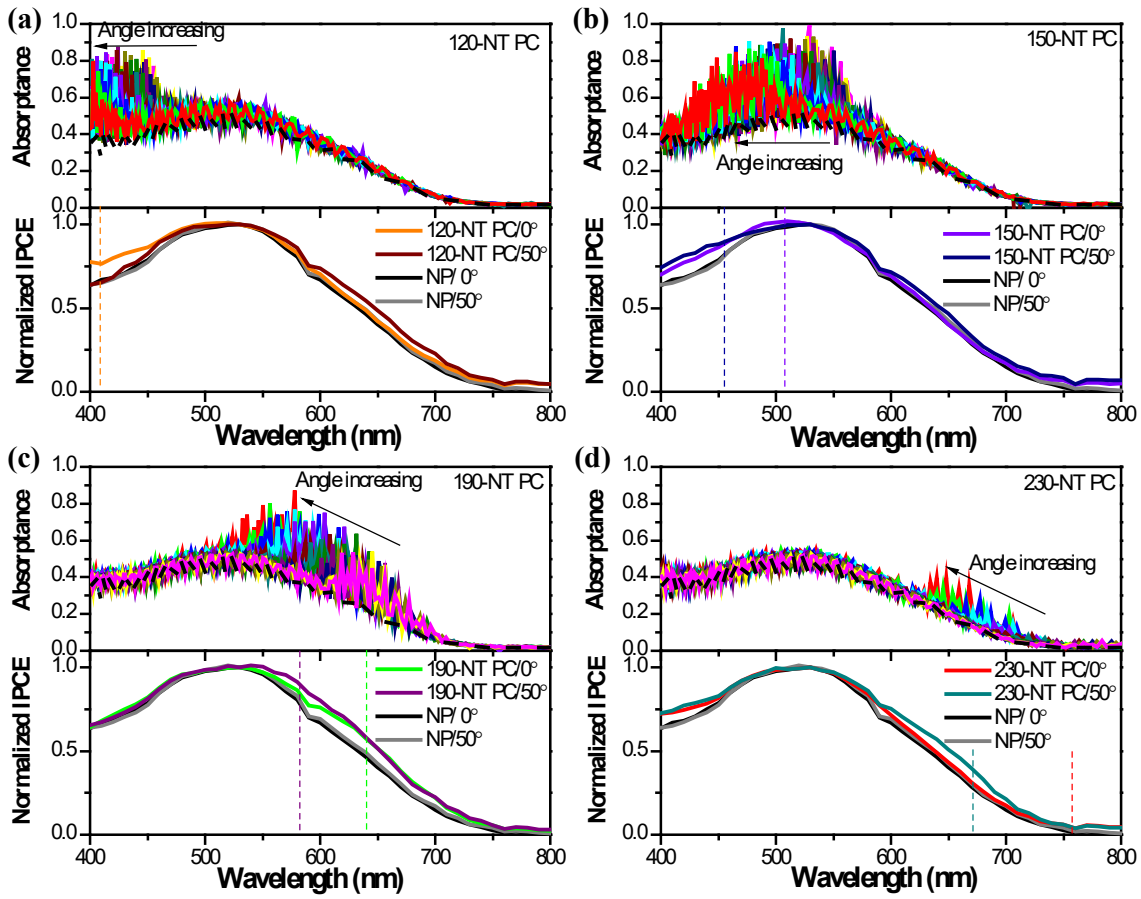

Fig. 5 Numerical simulated absorptance (top figure) and normalized IPCE (bottom figure) of the DSSCs coupled with different TiO_2 NT PCs, under an incident angle of 0 and 50°: (a) 120-NT PC, (b) 150-NT PC, (d) 190-NT PC and (d) 230-NT PC. All the experimental spectra are normalized at a wavelength of 530 nm. The curves from an NP-based reference DSSC are also plotted for comparison. The vertical dashed lines show the Bragg positions at the incident angle of 0 and 50°.

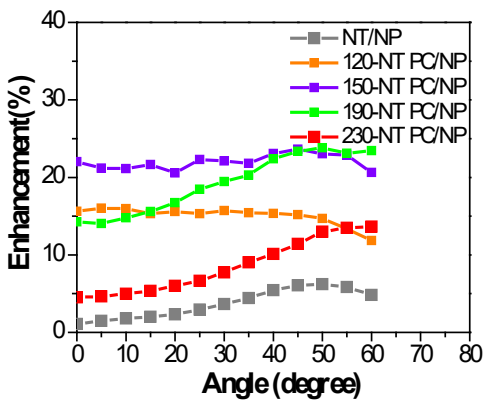

Fig. 6 The calculated ΔJsc (according to Eq. 1) of different types of DSSCs, as a function of incident angle.

NTs enhances the IPCE in the whole spectrum range, as can be seen from the simulated absorption spectra of TiO_2 NT coupled DSSC (Figure S7). These results are in good agreement with the afore-mentioned angular response of photocurrent of those TiO_2 NT PC coupled DSSCs. The ΔJ_{sc} calculated from the simulated absorptance of cells using Eq. 1 is displayed in Figure 6, which agrees well with the experimental result (Figure 4c).

Figure 7 shows the simulated 2D electric field distribution in each layer of DSSC coupled with 190-NT PC under incident angle of 0° and 50° for two selected wavelengths. It can be seen from Figure 7 that, for the wavelength of 640 nm, the Bragg mirror behavior of the NT PC causes a rapid electric field reduction in the PC layer and a strong electric field localization in the NP absorbing layer. This phenomenon disappears when

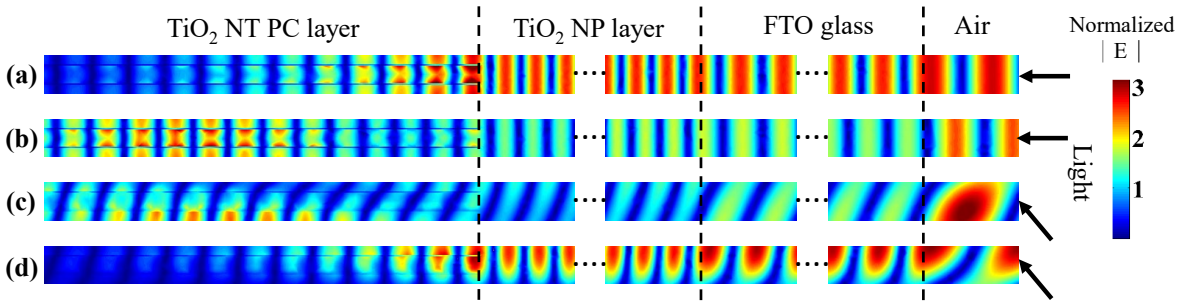

Fig. 7 The simulated 2D distribution of the electric field in each layer of DSSC coupled with 190-NT PC under the incident angle of 0 and 50° for two selected wavelengths. The incident angle and wavelength used in each graph are (a) 0°, 640 nm; (b) 0°, 590 nm; (c) 50°, 640 nm; and (d) 50°, 590 nm, respectively.

the incident angle is increased to 50°, due to the blue shift of the Bragg position of the NT PC. However, as shown in Figure 7d, this phenomenon reappears at a shorter wavelength of 590 nm, when the incident angle is 50°.

Conclusions

The angular response of the optical properties of TiO_2 NT PC and the performances of the corresponding integrated DSSCs were systemically studied. We have demonstrated that the introduction of TiO_2 NT PC with various lattice constants, ranging from 120 to 230 nm not only produces a significant photocurrent enhancement under normally incident light, but also maintains a stable power output when the incident light is tilted from 0° to 60°. The angular dependence of the enhancement effect and the photocurrent revealed a distinct evolution, which has been discussed with both experimental and simulated methods. For the TiO_2 NT PCs with a Bragg position at the blue side of the dye absorption peak, the angular evolution of J_{sc} show a trend similar to that of the TiO_2 NP based DSSCs, due to the compromise between a weaker peak overlap (overlap of the Bragg and dye absorption peaks) and a stronger light scattering; whereas, for the TiO_2 NT PCs with a Bragg position on the red side, both the stronger peak overlap and the light scattering lead to a slower drop in J_{sc} with respect to the incident angle. Our results showed that, by making use of the blue shift of the Bragg peak and the enhanced light scattering from TiO_2 NT PC under oblique incidence, the photovoltaic performance of DSSCs can be made less sensitive to irradiance, an attractive feature for applications. It is believed that our work presented here offers new insight and guidance to the design and application of photonic crystals to optoelectronic devices that are irradiance sensitive.

Acknowledgements

This work was supported by grants received from the Research Grants Council of the Hong Kong Special Administrative Region (Project Nos. PolyU5159/13E and PolyU5163/12E) and the Hong Kong Polytechnic University (Project No. RT5W). Keyu Xie is also grateful for the financial support from the National Natural Science Foundation of China (No.51302219), and the Specialized Research Fund for the Doctoral Program of Higher Education of China (No.20136102120024 and 20136102140001).

Notes and references

[a] Department of Applied Physics and Materials Research Center, The Hong Kong Polytechnic University, Hong Kong, China.
E-mail: aphhuang@polyu.edu.hk
[b] State Key Laboratory of Solidification Processing and Center for Nano Energy Materials, Northwestern Polytechnical University, Xi'an, China.
[c] Department of Mechanical Engineering, The Hong Kong Polytechnic University, Hong Kong, China.
E-mail: kyxie@nwpu.edu.cn

† Electronic Supplementary Information (ESI) available: [details of any supplementary information available should be included here]. See DOI: 10.1039/b000000x/

1 M. L. Brongersma, Y. Cui, S. Fan, *Nat. Mater.* 2014, **13**, 451.
2 S. Mathew, A. Yella, P. Gao, R. Humphry-Baker, B. F. Curchod, N. Ashari-Astani, I. Tavernelli, U. Rothlisberger, M. K. Nazeeruddin, M. Gratzel, *Nat. Chem.* 2014, **6**, 242.
3 L. Dominici, L. Vesce, D. Colonna, F. Michelotti, T. M. Brown, A. Reale, A. Di Carlo, *Applied Physics Letters* 2010, **96**, 103302.
4 B. Lipovšek, J. Krč, M. Topič, Senior Member, IEEE, *IEEE Journal of Photovoltacics* 2014, **4**, 936.
5 A. Kay, M. Gräitzel, *Sol. Energ. Mat. Sol. Cells* 1996, **44**, 96.

6 W. Hou, P. Pavaskar, Z. Liu, J. Theiss, M. Aykol, S. B. Cronin, *Energy Environ. Sci.* 2011, **4**, 4654.

7 S. K. Karuturi, J. Luo, C. Cheng, L. Liu, L. T. Su, A. I. Y. Tok, H. J. Fan, *Adv. Mater.* 2012, **24**, 4157.

8 M. Ye, H. Y. Liu, C. Lin, Z. Lin, *Small* 2013, **9**, 312.

9 A. Hinsch, W. Veurman, H. Brandt, K. F. Jensen, S. Mastroianni, *Chemphyschem* 2014, **15**, 1076.

10 J. H. Yum, E. Baranoff, F. Kessler, T. Moehl, S. Ahmad, T. Bessho, A. Marchioro, E. Ghadiri, J. E. Moser, C. Yi, M. K. Nazeeruddin, M. Grätzel, *Nat. Commun.* 2012, **3**, 631.

11 P. Routh, S. Das, A. Shit, P. Bairi, P. Das, A. K. Nandi, *ACS Appl. Mater. Interfaces* 2013, **5**, 12672.

12 N. Humphry-Baker, K. Driscoll, A. Rao, T. Torres, H. J. Snaith, R. H. Friend, *Nano Lett.* 2011, **12**, 634.

13 I. Chung, B. Lee, J. He, R. P. Chang, M. G. Kanatzidis, *Nature* 2012, **485**, 486.

14 C.-L. Wang, J.-Y. Hu, C.-H. Wu, H.-H. Kuo, Y.-C. Chang, Z.-J. Lan, H.-P. Wu, E. Wei-Guang Diau, C.-Y. Lin, *Energy Environ. Sci.* 2014, **7**, 1392.

15 J. Melas-Kyriazi, I. K. Ding, A. Marchioro, A. Punzi, B. E. Hardin, G. F. Burkhard, N. Tétreault, M. Grätzel, J.-E. Moser, M. D. McGehee, *Adv. Energy Mater.* 2011, **1**, 407.

16 A. Dualeh, T. Moehl, N. Tétreault, J. Teuscher, P. Gao, M.K. Nazeeruddin, M. Gräitzel, *ACS Nano* 2014, **8**, 362.

17 L. Yang, B. Xu, D. Bi, H. Tian, G. Boschloo, L. Sun, A. Hagfeldt, E. M. J. Johansson, *J. Am. Chem. Soc.* 2013, **135**, 7378.

18 S. Colodrero, A. Mihi, L. Häggman, M. Ocaña, G. Boschloo, A. Hagfeldt, H. Míguez, *Adv. Mater.* 2009, **21**, 764.

19 C. Lopez-Lopez, S. Colodrero, M. E. Calvo, H. Miguez, *Energy Environ. Sci.* 2013, **6**, 1260.

20 S. Nishimura, N. Abrams, B. A. Lewis, L. I. Halaoui, T. E. Mallouk, K. D. Benkstein, J. van de Lagemaat, A. J. Frank, *J. Am. Chem. Soc.* 2013, **125**, 6306.

21 A. Mihi, C. Zhang, P. V. Braun, *Angew. Chem. Int. Ed.* 2011, **50**, 5712.

22 E. S. Kwak, W. Lee, N.-G. Park, J. Kim, H. Lee, *Adv. Funct. Mater.* 2009, **19**, 1093.

23 C. T. Yip, H. Huang, L. Zhou, K. Xie, Y. Wang, T. Feng, J. Li, W. Y. Tam, *Adv. Mater.* 2011, **23**, 5624.

24 M. Guo, K. Xie, J. Lin, Z. Yong, C. T. Yip, L. Zhou, Y. Wang, H. Huang, *Energy Environ. Sci.* 2012, **5**, 9881.

25 A. Mihi, H. Míguez, *J. Phys. Chem. B* 2005, **109**, 15968.

26 F. García-Santamaría, E. C. Nelson, P. V. Braun, *Phys. Rev. B* 2007, **76**, 075132.

27 A. Mihi, F. J. López-Alcaraz, H. Míguez, *Appl. Phys. Lett.* 2006, **88**, 193110

28 Standard spectrum taken from http://www.nrel.gov/rredc.

29 L. Liu, S. K. Karuturi, L. T. Su, A. I. Y. Tok, *Energy Environ. Sci.* 2011, **4**, 209.

30 J. Balenzategui, F. Chenlo, *Sol. Energ. Mat. Sol. Cells* 2005, **86**, 53

